The impact of design and operational parameters on the optimal performance of direct air capture units using solid sorbents

Adam Ward[1,2] · Maria M. Papathanasiou[1,2] · Ronny Pini[1]

Abstract

Direct capture of CO_2 from ambient air is technically feasible today, with commercial units already in operation. A demonstrated technology for achieving direct air capture (DAC) is chemical separation of CO_2 in a steam-assisted temperature-vacuum swing adsorption (S-TVSA) process. However, the potential to develop scalable solutions remains high, requiring a detailed understanding of the impact of both process design and operation on the performance of the DAC unit. Here, we address this knowledge gap by presenting a state-of-the-art process simulation tool for the purification of CO_2 from ambient air by a 5-step S-TVSA process. By considering the benchmark adsorbent APDES-NFC, we conduct multi-objective productivity/energy usage optimization of the DAC unit, subject to the requirement of producing a high purity CO_2 product ($\geq 95\%$). For the base case scenario, we find a maximum productivity of $\mathrm{Pr_{max}} = 6.20$ kg/m³/day and a minimum specific equivalent work of $\mathrm{W_{EQ,min}} = 1.66$ MJ/kg. While in reasonable agreement with published data, our results indicate that the description of both competitive adsorption and adsorption kinetics are key factors in introducing uncertainty in process model predictions. We also demonstrate that the application of formal optimization techniques, rather than design heuristics, is central to reliably assess the process performance limits. We identity that system designs employing moderate CO_2 sorption kinetics and contactors with low length-to-radius ratios yield the best performance in terms of system productivity. Finally, we find that moderate-high ambient relative humidities (50–75%) offer significantly favourable performance, and that a wide range of feed temperatures (5–30 °C) can be accommodated via process optimization without a significant impact on performance.

Keywords CO_2 capture · Process modelling · Process optimization · Gas adsorption

List of symbols

A	Antoine equation parameter (–)
b	Adsorption equilibrium constant (1/Pa)
b_0	Reference adsorption equilibrium constant (1/Pa)
B	Antoine equation parameter (°C)
c_G	GAB isotherm parameter (–)
c_M	GAB isotherm parameter (mol/kg)
$C_{p,g}$	Heat capacity of gas (J/mol/K)
$C_{p,s}$	Heat capacity of adsorbent (J/kg/K)
$C_{p,W}$	Heat capacity of column wall (J/kg/K)
C	Antoine equation parameter (°C)
D_L	Longitudinal dispersion coefficient (m²/s)
D_m	Molecular diffusivity (m²/s)
E_{ads}	Electrical energy usage of adsorption step (MJ)
E_{bd}	Electrical energy usage of blowdown step (MJ)
E_{des}	Electrical energy usage of desorption step (MJ)
E_{heat}	Electrical energy usage of heating step (MJ)
E_T	Specific electrical energy usage (MJ/kg)
h_{in}	Inside heat transfer coefficient (/m²/K/s)
h_{out}	Outside heat transfer coefficient (J/m²/K/s)
k_{CO_2}	CO_2 kinetic constant (1/s)
k_{H_2O}	CO_2 kinetic constant (1/s)
K_{ads}	GAB isotherm parameter (–)
K_Z	Thermal conductivity of gas (J/m/K/s)
K_W	Thermal conductivity of column wall (J/m/K/s)
L	Column length (m)

✉ Ronny Pini
r.pini@imperial.ac.uk

Adam Ward
adam.ward16@imperial.ac.uk

Maria M. Papathanasiou
maria.papathanasiou11@imperial.ac.uk

1 Department of Chemical Engineering, Imperial College London, London, UK

2 Sargent Centre for Process Systems Engineering, Imperial College London, London, UK

$m_{CO_2}^{prod}$	Mass of CO_2 produced during desorption step (kg)		T_j	Jacket temperature (K)
n_c	Number of components (–)		T_H	High temperature (K)
n_s	Saturation capacity of CO_2 (mol/kg)		T_L	Low temperature (K)
n_{s0}	Reference saturation capacity of CO_2 (mol/kg)		$\bar{v}$	Non-dimensional interstitial velocity (–)
$n_{CO_2}^{prod}$	Amount of CO_2 produced during desorption step (mol)		v_F	Air feed interstitial velocity (m/s)
			v_s	Steam feed interstitial velocity (m/s)
$n_{H_2O}^{prod}$	Amount of water produced during desorption step (mol)		v_0	Characteristic interstitial velocity (m/s)
			V_{bed}	Volume of adsorption bed (m³)

$m_{CO_2}^{prod}$ — Mass of CO_2 produced during desorption step (kg)

n_c — Number of components (–)

n_s — Saturation capacity of CO_2 (mol/kg)

n_{s0} — Reference saturation capacity of CO_2 (mol/kg)

$n_{CO_2}^{prod}$ — Amount of CO_2 produced during desorption step (mol)

$n_{H_2O}^{prod}$ — Amount of water produced during desorption step (mol)

$n_{N_2}^{prod}$ — Amount of N_2 produced during desorption step (mol)

$n_{H_2O}^{in,des}$ — Amount of steam fed during desorption step (mol)

p — Pressure (Pa)

$\bar{p}$ — Non-dimensional pressure (–)

p_{CO_2} — Partial pressure of CO_2 (Pa)

p_{H_2O} — Partial pressure of water (Pa)

$p_{H_2O}^*$ — Vapor pressure of water (Pa)

p_0 — Characteristic pressure (Pa)

p_H — Ambient pressure (Pa)

Pe — Peclet number (–)

Pu_{CO_2} — CO_2 purity (%)

Pr — Productivity (kg/m³/day)

$q_{CO_2}^*$ — Specific adsorbed amount of CO_2 at equilibrium (mol/kg)

$q_{H_2O}^*$ — Specific adsorbed amount of water at equilibrium (mol/kg)

Q_{des}^{jacket} — Jacket heating of desorption step (MJ)

Q_{heat}^{jacket} — Jacket heating of heating step (MJ)

Q_{des}^{steam} — Heating to produce steam (MJ)

Q_{therm} — Specific thermal energy usage (MJ/kg)

r_H — Relative humidity (–)

r_{in} — Column innner radius (m)

r_{out} — Column outer radius (m)

r_p — Pellet radius (m)

SR — Steam ratio (–)

t — Time (s), or Toth exponent (–)

t_0 — Reference Toth exponent (–)

t_{ads} — Adsorption step duration (s)

t_{bd} — Blowdown step duration (s)

t_{cycle} — Total cycle duration (s)

t_{des} — Desorption step duration (s)

t_{heat} — Heating step duration (s)

t_{pres} — Pressurization step duration (s)

T — Temperature (K)

$\bar{T}$ — Non-dimensional temperature (–)

$\bar{T}_j$ — Non-dimensional jacket temperature (–)

$\bar{T}_W$ — Non-dimensional wall temperature (–)

T_0 — Reference temperature (K)

T_a — Ambient temperature (K)

T_j — Jacket temperature (K)

T_H — High temperature (K)

T_L — Low temperature (K)

$\bar{v}$ — Non-dimensional interstitial velocity (–)

v_F — Air feed interstitial velocity (m/s)

v_s — Steam feed interstitial velocity (m/s)

v_0 — Characteristic interstitial velocity (m/s)

V_{bed} — Volume of adsorption bed (m³)

W_{EQ} — Specific equivalent work (MJ/kg)

W_{min} — Minimum specific equivalent work (MJ/kg)

x — Non-dimensional adsorbed amount (–)

x^* — Non-dimensional adsorbed amount at equilibrium (–)

y_{H_2O} — Mole fraction of water (–)

$y_{CO_2,F}$ — Mole fraction of CO_2 in feed (–)

$y_{H_2O,F}$ — Mole fraction of water in feed (–)

$y_{N_2,F}$ — Mole fraction of N_2 in feed (–)

Z — Non-dimensional axial coordinate (–)

Greek symbols

α — Toth temperature dependence parameter (–), or dimensionless group (–)

β — Toth co-adsorption parameter (kg/mol)

γ — Toth co-adsorption parameter (kg/mol)

ΔH_0 — Heat of adsorption (J/mol)

ϵ — Bed porosity (–)

η_{turb} — Isentropic turbine efficiency (–)

θ — Vector of operating conditions

θ_L — Vector of operating condition lower bounds

θ_U — Vector of operating condition upper bounds

μ — Viscosity (kg/m/s)

μ_{2law} — Second law efficiency (–)

Π_1 — Dimensionless group (–)

Π_2 — Dimensionless group (–)

Π_3 — Dimensionless group (–)

ρ_b — Bed density (kg/m³)

ρ_W — Column wall density (kg/m³)

σ — Dimensionless group (–)

τ — Non-dimensional time (–), or column aspect ratio (–)

ϕ — Penalty function

χ — Toth temperature dependence parameter (–)

ψ — Dimensionless group (–)

Ω_1 — Dimensionless group (–)

Ω_2 — Dimensionless group (–)

Ω_3 — Dimensionless group (–)

Ω_4 — Dimensionless group (–)

Abbreviations

CSS — Cyclic steady state

DAC — Direct air capture

GAB — Guggenhein–Anderson de Boer

GGR — Greenhouse gas removal

NSGA-II	Non-dominated sorting genetic algorithm II
ODE	Ordinary differential equation
PDE	Partial differential equation
S-TVSA	Steam-assisted temperature-vacuum swing adsorption
TVSA	Temperature-vacuum swing adsorption
WENO	Weighted essentially non-oscillatory

1 Introduction

It is now broadly recognised that greenhouse gas removal (GGR) will play an important role in our transition to a net-zero society [1, 2]. GGR allows for the handling of hard-to-abate residual emissions, decentralized emissions, and historical emissions of CO_2. Among the available options for achieving GGR, direct removal of CO_2 from the atmosphere by direct air capture (DAC) is a leading technological solution [3–5]. In a DAC process, ambient air from the atmosphere is taken as a feed stream and CO_2 is removed by chemical separation, yielding a CO_2-lean air stream, which can be returned to the atmosphere, and a high purity CO_2 stream. The latter can be sent downstream to be stored permanently in underground geological formations [6], or for use as a chemical feedstock for the production of, e.g., carbon-based fuels [7, 8]. Therefore, DAC can be used to provide net CO_2 removal from the atmosphere (in the case of geological CO_2 storage), or to provide a means by which to utilize carbon-based fuels with near net-zero carbon emissions along the entire value chain (in the case of CO_2 utilisation) [9].

A leading technology for performing DAC is chemical separation by adsorption onto porous solids [10, 11]. Particularly, previous academic studies [12–16] and industrial patent applications [17, 18] have shown that a steam-assisted temperature-vacuum swing adsorption (S-TVSA) process is capable of producing high purity CO_2 ($\geq$ 95%) from ambient air. In an S-TVSA process, CO_2 is adsorbed from air onto the surface of an adsorbent solid at ambient pressure and temperature. Subsequently, the pressure of the bed is lowered and the temperature is increased using a steam purge to release CO_2 from the solid surface, in a controlled manner, at high purity. The process cycles between adsorption and regeneration modes, capturing CO_2 from the air in a semi-batch fashion. In practice, the design of adsorption-based processes is challenging owing to the strongly non-linear mass and heat transfer dynamics which occur inside the adsorption column [19]. The relationship between operational decisions, such as the duration of each step in the cycle, as well as the operating temperatures/pressures and gas flow rates, is complex with respect to metrics of the process performance. Specifically, we aim to make operational decisions such that we are able to achieve a high system productivity, while requiring a low electrical and thermal
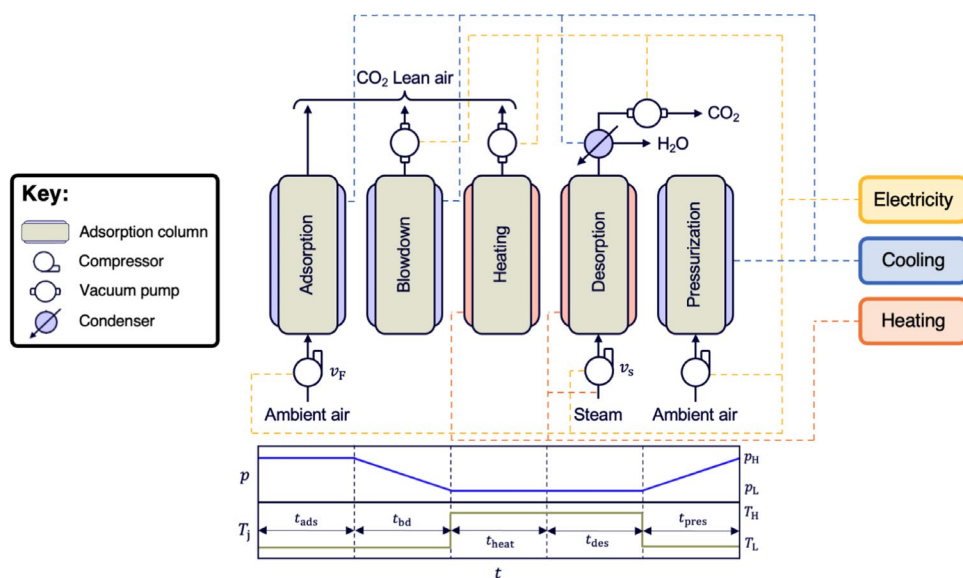
energy demand [20, 21] and achieving high CO_2 purity in the product stream.

There currently exist only a handful of process modelling studies of fixed-bed S-TVSA for DAC. Notably, this previous work has conducted the design of the process cycle according to heuristic guidelines with respect to the cycling times, operating pressures/temperatures, gas flowrates, and contactor design [14–16]. While practical, this approach does not yield a near-optimal process design owing to the complex dynamics of cyclic adsorption systems. As such, opportunities exist for substantial performance improvements via formal process optimisation approaches. Moreover, while previous work has elucidated the local [14, 15] or global [16] sensitivity of the process performance to various design parameters, the comparison of different design cases remains elusive, as these do not represent the best-case of process performance under each set of operating conditions. We also note that previous studies have all evaluated the performance of the adsorption process by calculating the performance indicators considering the product gas stream on a dry basis. However, the product gas from an S-TVSA process contains a significant amount of water vapor, so accounting accurately for the downstream condensation of water is essential for achieving an accurate characterization of the system performance.

In this work, we present a rigorous and computationally efficient framework for the simulation and optimization of DAC by an S-TVSA process. We evaluate the performance of the process by finite volume simulation of the fundamental material, momentum, and energy balance equations which govern the dynamics of a fixed-bed adsorption column. We explicitly account for the downstream separation of CO_2/H_2O in a single-stage condensation unit via thermodynamic modelling to allow for accurate determination of the purity of the CO_2 product. We apply this framework to the design of the S-TVSA process using a fixed-bed of the benchmark APDES-NFC adsorbent. As such, a central aim of this work is to rationalise the observed variability in the process performance metrics in terms of productivity and energy usage reported for both traditional TVSA processes [20, 22] and steam-assisted S-TVSA processes [14] using the same adsorbent. To this end, we have formally optimized the system performance through the application of a black-box population-based genetic algorithm to maximize the system productivity and minimize the system energy usage, while achieving high CO_2 purity ($\geq$ 95%). Finally, we study the impact of feed conditions (temperature and relative humidity), CO_2 kinetics, and contactor design on the performance of the S-TVSA process by optimizing the process operating conditions under a wide range of design scenarios.

The remainder of the study is organised as follows. In the methods Section, we describe the simulation and optimization framework which we have developed and deployed for

the analysis of the 5-step S-TVSA process. In the results Section, we present the outcome of the system optimization and make recommendations for the design of such systems in practice. Finally, in the discussion Section, we analyse the effect of key factors on the design of the system, particularly, the ambient feed conditions, the CO_2 adsorption kinetics, and the contactor design.

2 Methods

2.1 Temperature-vacuum swing adsorption cycle

In this work, we consider the separation of CO_2 from a humid air stream comprising CO_2, N_2 and H_2O with a pressure of $p = 1$ bar, a temperature of $T = 20\,°C$, a CO_2 concentration of 400 ppm, and a relative humidity of $r_H = 50\%$. We consider a fixed bed adsorption process utilizing a packed bed of APDES-NFC adsorbent [23]. APDES-NFC is an amine functionalized chemisorbent polymer, which has been shown in previous studies to have favourable adsorption equilibrium and kinetic properties for use in DAC processes [23–25]. We consider a steam-assisted temperature-vacuum swing adsorption process for DAC [14, 16]. A schematic representation of the process cycle is provided in Fig. 1. The cycle comprises five steps; (1) adsorption, (2) blowdown, (3) heating, (4) desorption, and (5) pressurization. In the adsorption step, ambient air is introduced to the column from the feed end. In this step, CO_2 and H_2O co-adsorb onto the surface of the solid, and a CO_2-lean air stream is eluted from the product end of the column. In the blowdown step, the pressure of the column is reduced using a vacuum pump. The aim of this step is to remove residual N_2 which is accumulated

in the inter-pellet void space in the column at the end of the adsorption step. In the heating step, the temperature in the heating jacket is increased to pre-heat the bed in preparation for the desorption step, while maintaining the vacuum level in the column using the vacuum pump. In the desorption step, a steam purge is introduced to the column from the feed end. The gas eluted from the product end during this step is predominantly a mixture of CO_2 and H_2O. The product gas is sent through a condenser to remove water and yield a high purity stream of CO_2. Finally, in the pressurization step, the pressure of the column is increased by introducing ambient air to the column from the feed end, with the product end closed. During this step, cooling water is introduced to the jacket to return the column to ambient temperature in preparation for the next adsorption cycle. The process continues to operate through the sequence of cycle steps, adsorbing and subsequently recovering CO_2 in a semi-batch fashion.

We note the following key features of the cycle just described. The pre-heating of the bed provides several important functions to the overall process. First, it allows for desorption to occur at a higher temperature, which is favourable for efficient release of CO_2 and H_2O. Second, it partially degasses the surface of the solid. Because the vacuum level inside the column is being maintained, this degassing process acts to further purge, by displacement, any residual N_2 from the bed which was not removed during the blowdown step—ensuring that the ultimate purity of the CO_2 product is high. Finally, pre-heating the bed acts to ensure that the temperature inside the column is sufficiently high as to avoid condensation of the steam purge inside the column during the subsequent desorption step. The steam acts to rapidly desorb CO_2 from the bed by two mechanisms. First, steam provides heat to the column
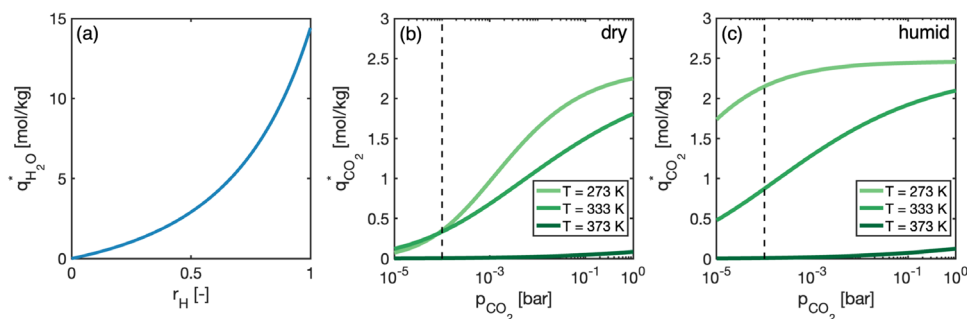
Fig. 2 CO_2/H_2O uptake on APDES-NFC adsorbent. **a** H_2O uptake as a function of relative humidity. **b** CO_2 uptake as a function of CO_2 partial pressure under dry conditions ($p_{H_2O} = 0$ Pa). **c** CO_2 uptake as a function of CO_2 partial pressure under humid conditions ($p_{H_2O} = 2550$ Pa). CO_2 isotherms are provided at three temperatures ($T = 293$ K, $T = 333$ K, $T = 373$ K). The vertical dashed line in panels (**b**) and (**c**) indicates the partial pressure of CO_2 in ambient air ($p_{CO_2} = 40$ Pa)

to overcome the chemical interactions formed between the solid and the gases during the adsorption step. Second, the flow of steam creates a displacement purge effect, whereby gas removed from the solid is rapidly swept away, maintaining a high driving force for mass transfer from the adsorbed-phase into the gas-phase.

2.2 Process simulation

2.2.1 Adsorption equilibrium

We calculate the adsorption equilibrium of CO_2/N_2/H_2O on the surface of APDES-NFC as a function of pressure, temperature, and gas-phase composition by using a combination of the Guggenhein–Anderson de Boer (GAB) and modified Toth isotherm models [14]. The adsorption of water on the surface of the solid is given by the GAB isotherm:

$$q^*_{H_2O} = \frac{c_M c_G K_{ads} r_H}{(1 - K_{ads})[1 + (c_G - 1)K_{ads} r_H]} \quad (1)$$

where $q^*_{H_2O}$ is the specific adsorbed amount of water, r_H is the relative humidity, and c_M, c_G and K_{ads} are empirical constants of the isotherm model. The relative humidity is calculated as the ratio of the partial pressure of water with its vapor pressure:

$$r_H = \frac{p_{H_2O}}{p^*_{H_2O}} = \frac{p y_{H_2O}}{p^*_{H_2O}} \quad (2)$$

where p is the total pressure, y_{H_2O} is the mole fraction of water, and $p^*_{H_2O}$ is the vapor pressure of water. The vapor pressure of water is calculated using Antoine's equation:

$$\log_{10}(p^*_{H_2O}) = A - \frac{B}{C + T} \quad (3)$$

where $p^*_{H_2O}$ is the vapor pressure of water (mmHg), T is the temperature (°C), and A, B and C are empirical constants. The adsorption of CO_2 on the surface of the solid has been described using a modified Toth isotherm model:

$$q^*_{CO_2} = \frac{n_s b p_{CO_2}}{\left[1 + \left(b p_{CO_2}\right)^t\right]^{1/t}} \quad (4)$$

where $q^*_{CO_2}$ is the specific adsorbed amount of CO_2, $p_{P_{CO_2}}$ is the partial pressure of CO_2, n_s is the saturation capacity of CO_2 on the surface, b is the adsorption equilibrium constant, and t is the Toth exponent. The isotherm parameters are expressed as functions of the temperature and specific water loading, as follows:

$$n_s = n_s(T, q^*_{H_2O}) = \left[\frac{1}{1 - \gamma q^*_{H_2O}}\right] n_{s0} \exp\left[\chi\left(1 - \frac{T}{T_0}\right)\right] \quad (5)$$

$$b = b(T, q^*_{H_2O}) = \left[1 + \beta q^*_{H_2O}\right] b_0 \exp\left[\frac{-\Delta H_0}{RT_0}\left(1 - \frac{T_0}{T}\right)\right] \quad (6)$$

$$t = t(T) = t_0 + \alpha\left(1 - \frac{T_0}{T}\right) \quad (7)$$

The adsorption isotherms of H_2O and CO_2 are provided in Fig. 2. We can see that the presence of moisture on the amine functionalised surface acts to increase both the maximum capacity of the sorbent for CO_2, as well as the steepness of the isotherm in the low pressure region. The latter is a key requirement for achieving high CO_2 uptake at the very low partial pressure of CO_2 which is present in ambient air. In accordance with previous studies on chemisorbents for DAC, we have assumed that the surface of APDES-NFC is effectively inert to N_2 [11]. This characteristic of the material

Table 1 Parameters of the GAB isotherm and modified Toth isotherm models for the adsorption of CO_2/H_2O on the surface of APDES-NFC adsorbent [14], and parameters of Antoine's equation for the vapour pressure of water

Parameter	Value	Units
GAB isotherm		
c_M	36.48	(mol/kg)
c_G	0.1489	(–)
K_{ads}	0.5751	(–)
Antoine's equation		
A	8.07131	(–)
B	1730.63	(°C)
C	233.426	(°C)
Toth isotherm		
T_0	296	(K)
n_{s0}	2.38	(mol/kg)
b_0	70.7	(kPa^{-1})
t_0	0.4148	(–)
ΔH_0	− 57.047	(kJ/mol)
α	− 1.606	(–)
χ	0	(–)
γ	0.0016	(kg/mol)
β	59.1	(kg/mol)

makes it a good choice for the removal of ultra-dilute CO_2 from ambient air, by providing an effective bulk separation between CO_2 and N_2. The parameters of the GAB isotherm, Antoine's equation, and the modified Toth isotherm which have been used in this work for predicting the adsorption equilibrium in the system are provided in Table 1.

2.2.2 Adsorption dynamics

The dynamics taking place inside the packed bed adsorption column have been described using a 1D adsorption column model, which we developed during previous works [26, 27] and have adapted for the simulation of the S-TVSA process considered in this study. The model comprises a set of

material, momentum, and energy balance equations which account for the necessary mechanisms of mass and heat transfer in the adsorption process. The adsorption column model is a coupled system of partial differential equations, which are provided in non-dimensional form in Table 2. Definitions of the dimensionless groups in Table 2 are provided in Section S.1 of the Supporting Information. The overall and component material balances represent axially dispersed plug flow of an ideal gas mixture through the packed bed of adsorbent. This is coupled to an adsorption kinetics model which describes the transfer of species from the gas-phase to the adsorbed-phase as a first-order mass transfer process using the linear driving force approximation. The pressure drop equation relates the pressure to the gas flow rate using Darcy's law for flow in a packed bed of spherical pellets. There are energy balance equations for both the gas-phase temperature, and the temperature of the column wall. The energy balance equations account for all key heat transfer mechanisms taking place in the system, including; conduction, convection, heat released by exothermic adsorption, and heat exchanged with the heating jacket.

2.2.3 Finite volume simulation

The 5-step adsorption process described in Sect. 2.1 has been simulated by numerical solution of the material, momentum, and energy balance equations comprising the adsorption dynamics model (Table 2) using a finite volume approach. The model equations are a coupled set of partial differential equations (PDEs) describing the variation of the state of the system in both space and time. First, the equations are discretized in space by dividing the column into 10 volume elements using a weighted essentially non-oscillatory (WENO) finite volume scheme [19]. This results in a system of coupled ordinary differential equations describing the evolution of the state of the system with time. The system of ordinary differential equations (ODEs) has been integrated with respect to time using the *ode15s* solver in

Table 2 The system of non-dimensional partial differential equations representing the material, momentum, and energy balances of the 1D adsorption dynamics model

Overall material balance	$\frac{\partial \bar{p}}{\partial \tau} - \frac{\bar{p}}{\bar{T}}\frac{\partial \bar{T}}{\partial \tau} = -\bar{T}\frac{\partial}{\partial Z}\left(\frac{\bar{p}\bar{v}}{\bar{T}}\right) - \psi\bar{T}\sum_{i=1}^{n_c}\frac{\partial x_i}{\partial \tau}$
Component material balance	$\frac{\partial y_i}{\partial \tau} + \frac{y_i}{\bar{p}}\frac{\partial \bar{p}}{\partial \tau} - \frac{y_i}{\bar{T}}\frac{\partial \bar{T}}{\partial \tau} = \frac{1}{Pe}\frac{\bar{T}}{\bar{p}}\frac{\partial}{\partial Z}\left(\frac{\bar{p}}{\bar{T}}\frac{\partial y_i}{\partial Z}\right) - \frac{\bar{T}}{\bar{p}}\frac{\partial}{\partial Z}\left(\frac{y_i\bar{p}\bar{v}}{\bar{T}}\right) - \frac{\bar{T}}{\bar{p}}\psi\frac{\partial x_i}{\partial \tau}$
Solid-phase material balance	$\frac{\partial x_i}{\partial \tau} = \alpha_i(x_i^* - x_i)$
Pressure drop	$-\frac{\partial \bar{p}}{\partial Z} = \frac{150}{4r_p^2}\left(\frac{1-\epsilon}{\epsilon}\right)^2\frac{v_0 L}{p_0}\mu\bar{v}$
Column energy balance	$\frac{\partial \bar{T}}{\partial \tau} + \Omega_2\frac{\partial \bar{p}}{\partial \tau} = \Omega_1\frac{\partial^2 \bar{T}}{\partial Z^2} - \Omega_2\frac{\partial}{\partial Z}(\bar{p}\bar{v}) + \sum_{i=1}^{n_c}\left[(\sigma_i - \Omega_3\bar{T})\frac{\partial x_i}{\partial \tau}\right] - \Omega_4(\bar{T} - \bar{T}_w)$
Wall energy balance	$\frac{\partial \bar{T}_w}{\partial \tau} = \Pi_1\frac{\partial^2 \bar{T}_w}{\partial Z^2} + \Pi_2(\bar{T} - \bar{T}_w) - \Pi_3(\bar{T}_w - \bar{T}_j)$

Definitions of the symbols used in this Table can be found in the Nomenclature Section. Definitions of the dimensionless groups used in this Table can be found in Section S.1 of the Supporting Information file

MATLAB. To allow for efficient solution of the model, the equations are solved in a non-dimensional form. Further, we also supply the ODE solver with the Jacobian sparsity pattern of the system. The time derivatives of the states of the system are co-dependant, which we handle in the solution by applying a mass matrix approach. The absolute and relative tolerances of the ODE solver were both set at 10^{-6}.

The equations are integrated subject to boundary conditions representing the 5-step adsorption cycle described in Sect. 2.1. The boundary conditions used to represent each step are provided in Section S.2 of the Supporting Information. The adsorption process operates cyclically through the cycle steps. Therefore, the model equations must be integrated repeatedly through the cycle steps until the attainment of a cyclic steady state (CSS). We have defined the attainment of CSS as a change of less than 0.5% between the beginning and end of a cycle in the pressure, temperature, gas-phase composition, adsorbed amount, and wall temperature at any position in the column [16]. Once CSS has been attained, we calculate the key performance indicators of the process performance using the column profiles at CSS. The initial condition of the column at the beginning of a simulation is that the column is filled with N_2 at ambient temperature and pressure. Then, the initial condition for each successive cycle step is taken as the final state of the column from the preceding step.

The numerical implementation of the S-TVSA process simulator has been validated by comparison to simulation results available in the literature [14]. The process simulator has been found to be in strong agreement with the literature simulation, and the results of the validation exercise can be found in Section S.3 of the Supporting Information.

2.2.4 Downstream process equipment

Downstream of the column during the desorption step, there is a condenser for the removal of water from the product gas to allow for the production of a high-purity CO_2 stream. Previous work on the simulation of steam-assisted adsorption-based DAC processes has assumed that the condenser achieves total condensation of all water eluted from the column during the desorption step [14–16]. However, we note that the amount of water which can be condensed is inherently limited by the thermodynamic equilibrium between water and CO_2 at the operating conditions of the condenser, as governed by the vapour pressure of water at a given temperature. Because the amount of water produced during the desorption step is typically more than an order of magnitude larger than the amount of CO_2 produced, even a highly effective condenser may leave a large residual amount of water in the product stream relative to the amount of produced CO_2. As such, it is important to account for the actual achievable separation of these components downstream of the column

when calculating the process key performance indicators. Further, we note that CO_2 is soluble in water, which will lead to some amount of loss of the CO_2 product to dissolution in the condensed phase inside the condenser. It has also been shown experimentally in previous work that the discharge of the product stream through the vacuum pump to atmospheric conditions causes further condensation of water from the product stream [28]. Therefore, to account for these effects, we have employed a thermodynamic model for the condenser and vacuum pump downstream of the column during the desorption step. Full details of the thermodynamic model, and the associated solution procedure, are provided in Section S.4 of the Supporting Information file. The condenser operates under vacuum at a pressure $p_1 = p_L$ and a temperature $T_1 = 278\,\text{K}$. The vapour phase eluted from the condenser is fed to the vacuum pump, which discharges to atmospheric conditions $\left(p_2 = p_{\text{amb}}, T_2 = T_{\text{amb}}\right)$. We note that we trailed several possible configurations of the downstream process equipment before specifying the configuration described above. Details of the alternative configurations, and the selection process for the chosen configuration, are provided in Section S.5 of the Supporting Information.

2.2.5 Key performance indicators

We have quantified the performance of the adsorption process using four key performance indicators; the purity of the CO_2 product (Pu_{CO_2}), the productivity (Pr), the specific electrical energy usage (E_T), and the specific thermal energy usage (Q_{therm}). The purity of the CO_2 product extracted during the desorption step is calculated as:

$$\text{Pu}_{CO_2}\,(\%) = 100 \times \frac{n_{CO_2}^{\text{prod}}}{n_{CO_2}^{\text{prod}} + n_{H_2O}^{\text{prod}} + n_{N_2}^{\text{prod}}} \tag{8}$$

where n_i^{prod} is the number of moles of component i produced from the vacuum pump discharge during the desorption step. The productivity defines the capture rate of a given unit volume of the adsorption bed throughout the duration of a complete cycle. The productivity is calculated as:

$$\text{Pr}\,(\text{kg/m}^3/\text{day}) = \frac{m_{CO_2}^{\text{prod}}}{V_{\text{bed}} \cdot t_{\text{cycle}}} \tag{9}$$

where $m_{CO_2}^{\text{prod}}$ is the mass of CO_2 produced during the desorption step, $V_{\text{bed}} = \pi r_{\text{in}}^2 L$ is the volume of the adsorption bed, and $t_{\text{cycle}} = \sum_i t_i$ is the duration of a complete cycle. The electrical energy usage of the process is the sum of the energy required to run the compressor for open flow during the adsorption and desorption steps, respectively, with the energy required to run the vacuum pump to pull and hold vacuum during the blowdown and heating steps,

respectively. Therefore, the specific electrical energy usage is calculated as:

$$E_{elec} \, (MJ/kg) = \frac{E_{ads} + E_{bd} + E_{heat} + E_{des}}{m_{CO_2}^{prod}} \quad (10)$$

where E_i is the electrical energy usage of step i. We note that no electrical energy is consumed for re-pressurization of the column following the desorption step, as the feed stream is available at the desired high pressure of the process (i.e. ambient conditions). The thermal energy usage of the process is the sum of the heating required from the heating jacket during the heating and desorption steps, and the heating required to produce steam for the desorption step. Therefore, the specific thermal energy usage is calculated as:

$$Q_{therm} \, (MJ/kg) = \frac{Q_{heat}^{jacket} + Q_{des}^{jacket} + Q_{des}^{steam}}{m_{CO_2}^{prod}} \quad (11)$$

where Q_i^{jacket} is the heat required in the jacket for step i, and Q_{des}^{steam} is the heat required to produce steam for the desorption step. As an additional metric for assessing the thermal requirements of the process, we also calculate the steam ratio, which we define as:

$$SR \, (-) = \frac{n_{H_2O}^{in,des}}{n_{CO_2}^{prod}} \quad (12)$$

where SR is the steam ratio (i.e. moles of steam required per mole of CO_2 captured), and $n_{H_2O}^{in,des}$ is the amount of steam fed to the column during the desorption step. To allow for the expression of the total energy duty of the capture process as a single value for the purposes of process optimization, we have adopted the concept of the specific equivalent work to lump the electrical and thermal energy usage [29]. The specific equivalent work is calculated as [30]:

$$W_{EQ} \, (MJ/kg) = E_{elec} + \eta_{turb}\left(1 - \frac{T_L}{T_H}\right)Q_{therm} \quad (13)$$

where η_{turb} is the turbine isentropic efficiency of a hypothetical turbine undertaking the conversion between electrical and thermal work. Here, we have assumed an isentropic efficiency of $\eta_{turb} = 0.75$ [29]. Finally, a useful concept for analysing the energy efficiency of carbon capture processes is the thermodynamic second law efficiency, which is defined as [31]:

$$\mu_{2law} \, (\%) = 100 \times \frac{W_{min}}{W_{EQ}} \quad (14)$$

where μ_{2law} is the second law efficiency, and W_{min} is the theoretical minimum work associated with the separation.

The actual work required for the separation (W_{EQ}) is always greater than the theoretical minimum work (W_{min}), therefore the second law efficiency is in the range $\mu_{2law} \in [0, 100]\%$. It has been estimated that the minimum work for a DAC process (assuming a capture rate of 75%) is $W_{min} = 0.468$ MJ/kg, and that the corresponding second law efficiency for practical processes is approximately 10–30% (i.e. the separation requires approximately 3–10x the theoretical minimum energy usage) [20, 31].

Full details of the calculation of each of the key performance indicators for the adsorption process described in this Section are provided in Section S.6 of the Supporting Information.

2.3 Multi-objective process optimization

We have optimized the performance of the DAC process described in Sect. 2.1 by maximizing the productivity of the system and minimizing the energy usage. The productivity represents a critical metric of the overall process performance, as it provides an indication of the system volume (and hence, land footprint), which is required to achieve a given CO_2 capture rate. Given the very large capture rates of DAC which need to be deployed globally to achieve meaningful climate impact (Gtns/yr by 2050, [2]), we would like the productivity of the system to be as high as possible to minimize the required land footprint. It has also been noted in a large body of previous literature that the energy usage of DAC processes is significant. We would therefore like to understand the minimum possible energy usage of a steam-assisted DAC process. Further, since both objectives are important, depending on contextual factors (e.g. regional availability of land and energy supplies), we would like to understand the trade-off between these two key metrics. Therefore, we have formulated the optimization of the system performance as a constrained multi-objective optimization problem with the following form:

$$\min_{\theta} \, \left[-Pr + \phi, \, W_{EQ} + \phi\right]$$
$$\text{s.t.} \quad \theta_L \leq \theta \leq \theta_U$$
$$\phi = 0.25 \times [\max(0, 95 - Pu_{CO_2})]^2$$

where θ is the vector of process operating variables, and θ_L and θ_U are the lower and upper bounds on the operating variables, respectively. We require that the purity of the CO_2 product is at least 95%, to ensure that the product stream is suitable for downstream geological sequestration, or for use as a chemical feedstock. The purity constraint is enforced using a quadratic loss penalty function approach, whereby we penalize solutions to the process model which do not satisfy the purity constraint by an amount proportional to the square of the violation of the constraint, represented by the

Table 3 Upper and lower bounds applied to the operating variables for optimization of the S-TVSA process

Parameter	t_{ads} (s)	t_{heat} (s)	t_{des} (s)	p_L (bar)	T_H (K)	v_s (m/s)	v_F (m/s)
Lower bound	1000	500	1000	0.05	363	0.0015	0.005
Upper bound	15,000	1500	40,000	0.5	373	0.005	0.01

penalty function, ϕ. The drawdown coefficient of the penalty function, $c = 0.25$, has been determined by a trial and error approach to ensure that the resulting solution is both efficient and appropriately constrained.

The upper and lower bounds used during optimization for the operating variables are provided in Table 3. As operating variables for the optimization, we have used the step durations of the adsorption (t_{ads}), heating (t_{heat}) and desorption (t_{des}) steps, the vacuum pressure (p_L), the steam temperature (T_H), the feed velocity of steam during desorption (v_s), and the feed velocity of air during adsorption (v_F). The duration of the blowdown (t_{bd}) and pressurization (t_{pres}) steps have both been fixed at 30 s. The input parameters used for simulation of the DAC process are provided in Table 4 [14].

The constrained multi-objective optimization problem has been solved using using the non-dominated sorting genetic algorithm II (NSGA-II). A large body of previous publications on the design of adsorption processes has shown that the NSGA-II algorithm is effective at solving for optimal process performance in terms of maximum productivity and minimum energy usage, in a variety of applications [19, 27, 32–35]. We have deployed an implementation of the NSGA-II algorithm available in the MATLAB Global Optimization Toolbox as the *gamultiobj* function. We apply the algorithm for 100 generations with a population size of 140. We have initialized the algorithm with an initial population of 140 operating points, and their corresponding key performance indicators, which were determined by quasi-random sampling using the Sobol sequence within the parametric bounds in Table 3. The optimization algorithm described in Sect. 2.3 is coupled to the process simulator described in Sect. 2.2 for calculation of the process performance indicators at specified sets of operating conditions.

Table 4 Parameters used for simulation of the 5-step S-TVSA process [14, 27]

Parameter	Value	Units
Column dimensions		
Column length, L	0.0181	(m)
Column inner radius, r_{in}	0.145	(m)
Column outer radius, r_{out}	0.162	(m)
Air feed conditions		
Ambient pressure, p_H	100,000	(Pa)
Ambient temperature, T_L	293	(K)
CO_2 mole fraction, $y_{CO_2,F}$	0.0004	(–)
H_2O mole fraction, $y_{H_2O,F}$	0.0115	(–)
N_2 mole fraction, $y_{N_2,F}$	0.9881	(–)
Physical properties		
Bed porosity, ϵ	0.37	(–)
Pellet radius, r_p	0.00375	(m)
Molecular diffusivity, D_m	1.6×10^{-5}	(m²/s)
Thermal conductivity of gas, K_z	0.09	(J/m/K/s)
Thermal conductivity of wall, K_w	16	(J/m/K/s)
Heat capacity of gas, $C_{p,g}$	42.46	(J/mol/K)
Heat capacity of wall, $C_{p,w}$	513	(J/kg/K)
Heat capacity of pellets, $C_{p,s}$	2000	(J/kg/K)
Bed density, ρ_b	55.4	(kg/m³)
Wall density, ρ_w	7800	(kg/m³)
Gas viscosity, μ	1.72×10^{-5}	(kg/m/s)
Transport parameters		
Longitudinal dispersion coefficient, D_L	$D_L = 0.7 D_m + v_F r_p$	(m²/s)
Inside heat transfer coefficient, h_{in}	3	(J/m²/K/s)
Outside heat transfer coefficient, h_{out}	26	(J/m²/K/s)
CO_2 mass transfer coefficient, k_{CO_2}	2×10^{-4}	(s⁻¹)
H_2O mass transfer coefficient, k_{H_2O}	2×10^{-3}	(s⁻¹)

3 Results

3.1 Process performance in optimized S-TVSA cycles

We have carried out constrained multi-objective optimization of an S-TVSA process utilizing a fixed bed of APDES-NFC adsorbent to find a Pareto front of maximum productivity and minimum energy usage, subject to the constraint that the CO_2 purity should be greater than 95%, according to the procedure set out in Sect. 2.3. The resulting Pareto front (orange symbols) is provided in Fig. 3. The dashed lines indicate the maximum productivity and minimum specific equivalent work values obtained by solving the corresponding constrained optimization problems in a single-objective mode. The maximum productivity of the process is calculated to be $Pr_{max} = 6.20$ kg/m³/day, and the minimum specific equivalent work of the process is calculated to be $W_{EQ,min} = 1.66$ MJ/kg. Between these extremes of performance, we observe a quasi-linear trade-off between productivity and energy usage. At the point of minimum energy usage, the specific equivalent work is comprised of 0.15 MJ/kg of electrical energy usage and 9.4 MJ/kg of
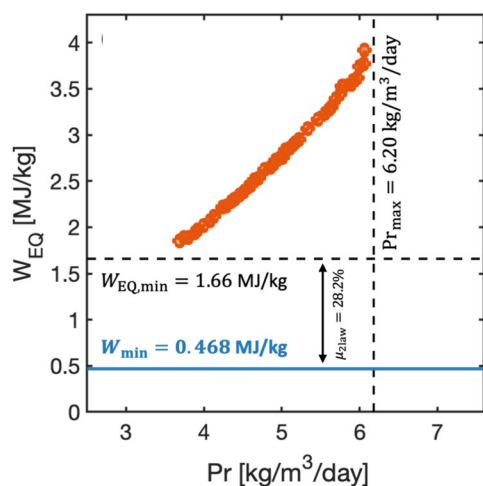
Fig. 3 Constrained productivity/energy usage Pareto front for the S-TVSA process. Orange symbols correspond to the multi-objective Pareto front calculated using the NSGA-II algorithm. Dashed lines correspond maximum productivity and minimum energy usage, respectively, calculated by single-objective optimization. Solid blue line corresponds to the theoretical minimum work for DAC [31] (Color figure online)

thermal energy usage (98.4% of total energy input utilized as heat). Based on this, and contrary to a significant body of previous research [11, 14, 16, 36], we contend that electrical energy usage (and hence, column pressure drop) is not a significant design limitation for S-TVSA DAC processes. In fact, we observe that prioritizing the reduction of the thermal energy usage will manifest as a much more effective strategy for reducing the overall energy burden. We suggest that a reduction in the thermal energy usage can be facilitated by adsorbent material innovations, through a combination of; (i) higher volumetric CO_2 capacity, (ii) lower heat of adsorption, and/or (iii) lower sorbent heat capacity—with properties (i) and (iii) targeting a reduction of the sorbent thermal mass within the adsorption column.

We can see in Fig. 3 that there is a strong agreement between the solutions to the corresponding single-objective optimization problems, and the extremes of the Pareto front obtained by multi-objective optimization. Relative to the highest productivity point on the Pareto front, the single-objective optimum represents an improvement of $\Delta Pr_{max} = +1.9\%$. Similarly, relative to the lowest energy usage point on the Pareto front, the single-objective optimum represents an improvement of $\Delta W_{EQ,min} = -10.2\%$. Therefore, while the multi-objective optimization is able to recover near-optimal extremes of performance, the results here underline the need to compute both single- and multi-objective solutions to the optimization problem if we wish to understand both the trade-off between the process objectives, and their possible minimum/maximum values. We note that when solving the multi-objective problem using

NSGA-II with settings for the algorithm adopted from our previous work (e.g. [27]), we found significant discrepancies between the extremes of the Pareto front and the corresponding single-objective optima. The number of generations and population size used for solution of the multi-objective optimization needed to be increased quite significantly in this work to recover near-optimal performance extremes via the Pareto front. This result highlights clearly the strongly non-linear nature of the design problem, which makes is rather challenging to solve relative to the design of adsorption-based systems in other gas separation applications.

3.2 Scalability of the DAC process

To provide context for the magnitude of the optimal process performance indicators obtained in the previous section, it is useful to make reference to optimized adsorption processes used in other carbon capture applications (e.g. post-combustion CO_2 capture). It is important to note that these applications of adsorption-based processes are not strictly comparable, as the process feed conditions are substantially different, and the two processes provide entirely distinct functions to the wider energy system. Nonetheless, the comparison aides in understanding where research efforts should be focused to improve the overall performance and scalability of the DAC process.

The calculated minimum specific equivalent work for the DAC system $\left(W_{EQ,min} = 1.66\,MJ/kg\right)$ represents a second law efficiency of $\mu_{2law} = 28.2\%$. Previous work has estimated that the second law efficiency for direct air capture lies approximately within the range $\mu_{2law} \approx 10–30\%$ [20, 31], indicating that the optimized S-TVSA process presented here represents an option for achieving DAC with strong efficiency in terms of energy usage. Applications of adsorption-based separations to post-combustion carbon capture ($y_{CO_2,F} = 3–30\%$) can achieve second law efficiencies of up to $\mu_{2law} \approx 30\%$ [31, 37], for designs that achieve a CO_2 recovery of at least 90%. Therefore, these results indicate that current adsorption-based technologies for DAC represent a relatively energy efficient approach, as we would typically anticipate that the second law efficiency of a carbon capture process is a decreasing function of the CO_2 feed composition. However, it is worth noting that while it possesses a similar second law efficiency, the DAC system presented here refers to a design that does not have an active constraint on the recovery.

With reference to the significant body of research on adsorption-based post-combustion CO_2 capture ($E_{min} \approx 150 –530\,kWh/tn$, [19, 27, 37]), the minimum energy usage of the S-TVSA process for DAC ($E_{min} \approx 461\,kWh/tn$) does not seem unreasonably large—despite previous literature emphasising significant concerns surrounding the energy requirements of DAC [3, 20, 38]. However, it must be

emphasised that achieving such an energy usage for the DAC process is accompanied by a very low system productivity, on the order of $\mathcal{O}(10^0)$ kg/m^3/day. Again, for reference, adsorption-based technology applied to post-combustion CO_2 capture can typically achieve an optimum productivity on the order of $\mathcal{O}(10^3$–$10^4)$ kg/m^3/day. We can use this comparison to understand that, indeed, the productivity of the S-TVSA process is extremely low. For example, we can estimate that processing, e.g., 1 Mtn/yr of CO_2 with such a unit would require approximately 600,000 m^3 of process volume, which is very large. We can therefore interpret from these results that to enable the deployment of DAC via S-TVSA processes at climate-relevant scales, significant efforts need to be dedicated towards improving the productivity of such systems, to allow for low land footprint requirements at large capture rates. Particularly, considering that DAC processes will likely be co-located to existing energy and carbon transport/storage infrastructure to enable strong environmental efficiency, land footprint is a significant concern [39]. With this in mind, in Sect. 4 we explore the effect of three key design parameters on the optimal productivity of the system; (i) the ambient feed conditions (temperature, relative humidity), (ii) the CO_2 kinetics, and (iii) the contactor design.

3.3 External bench-marking

In this Section, we provide an extensive bench-marking of the optimized process performance obtained in this work with external literature sources, including; (i) process design carried out according to heuristic design guidelines adopted in previous studies, (ii) performance metrics reported in previous academic studies for TVSA/S-TVSA processes utilizing APDES-NFC adsorbent, and (iii) estimated performance of a commercial demonstration unit operated by the company Climeworks.

In Fig. 4, the star symbol indicates the position in the Pareto plane of a design carried out according to heuristic guidelines adopted in previous studies (e.g. [14]). According to the heuristic design guidelines, the adsorption step duration (t_{ads}) is set such that the bed reaches 90% CO_2 saturation (relative to a fully regenerated bed), the heating time (t_{heat}) is set such that the bed is heated to a minimum of 5 °C above the boiling point of steam at the cycles low pressure (to prevent steam condensation during the desorption step), and the desorption time (t_{des}) is set to be approximately double that of the adsorption time. The air flowrate ($v_F = 0.0067$ m/s), steam flowrate ($v_s = 0.0034$ m/s), desorption pressure ($p_L = 0.05$ bar), and the steam temperature ($T_H = 368$ K) were fixed arbitrarily for the base-case design of the previous study, and these operating conditions have been adopted for the heuristic design case presented here. As we can see in Fig. 4, a substantial improvement in the system performance is achievable compared to the heuristic design, both in terms
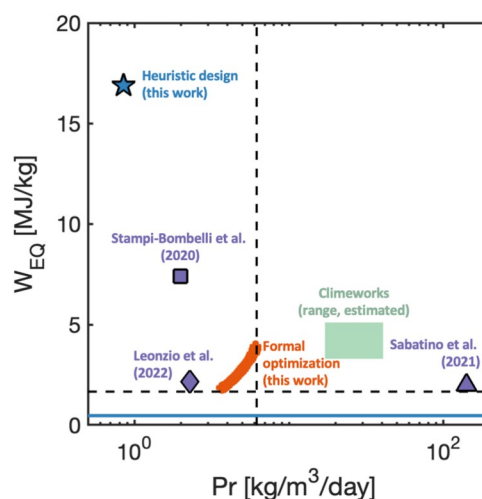

Fig. 4 Bench-marking of the process design results obtained in this work with various literature sources. Orange symbols correspond to the multi-objective Pareto front calculated using the NSGA-II algorithm (this work). Blue star corresponds to the process performance obtained when applying heuristic design guidelines from the literature (this work, see Sect. 3.3). Purple symbols correspond to the performance reported in literature [14, 20, 22]. Green shaded area corresponds to an estimated range of the performance of a 50 tn/yr Climeworks demonstration plant [20, 31] (Color figure online)

of productivity and energy usage, by applying formal optimization techniques to the design problem. We have observed a maximum productivity improvement of $\Delta Pr = +629\%$, and a maximum energy usage reduction of $\Delta W_{EQ} = -90.2\%$, as compared to the heuristic design case. It is therefore evident that the application of formal optimization techniques is central to accurate assessment of the performance limits of S-TVSA processes for DAC. A detailed discussion of the differences between the heuristic design and the design yielded from formal optimization in terms of the process operating conditions and system dynamics is provided in Sect. 3.4.

In Fig. 4, we also present the process performance reported in previous studies which utilize APDES-NFC adsorbent for DAC in TVSA/S-TVSA processes (square: [14], triangle: [20], diamond: [22]).

Sabatino et al. [20] carried out constrained multi-objective productivity/energy optimization for a TVSA process, and estimated the maximum productivity of the system to be 141 kg/m^3/day and the minimum specific exergy as 2 MJ/kg. The maximum productivity reported in this study is notably high when compared to other studies utilizing the same adsorbent. The same authors indicate that the observed discrepancy may be due to the very large values used for the kinetic constants of CO_2 $\left(k_{CO_2} = 0.1 \text{ s}^{-1}\right)$ and water $\left(k_{H_2O} = 1 \text{ s}^{-1}\right)$, which consequently yield very short cycle times ($t_{cycle} = 330$–450 s). By way of comparison, the cycle time reported for Climeworks's CO_2 collector is approximately 3. hrs [17], and the reported kinetics constants
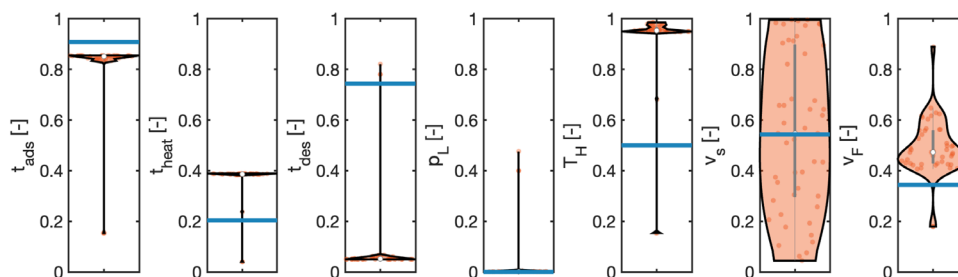
Fig. 5 Distributions of the process operating conditions on the Pareto front of the S-TVSA process. Orange violin plots correspond to the distributions of the operating conditions from the Pareto front in Fig. 3 determined using the NSGA-II algorithm. Solid blue lines cor-respond to the operating conditions from heuristic design. Each distribution has been re-scaled onto the interval [0, 1] according to the lower and upper bounds of each variable (see Table 3) (Color figure online)

used to model the unit are approx. $k_{CO_2} = 1 \times 10^{-3}\,\text{s}^{-1}$ and $k_{H_2O} = 1 \times 10^{-2}\,\text{s}^{-2}$, respectively [30]. Based on this, we conclude that CO_2 sorption kinetics represent a critical design parameter. However, we observe in the literature that sorption kinetics are scarcely measured in experimental studies on DAC adsorbents [11]. Therefore, in Sect. 4.2, we provide a parametric sensitivity analysis of the optimized system performance across a wide range of possible values for the CO_2 kinetic constant to study the impact of this parameter in detail.

Leonzio et al. [22] modelled a TVSA process employing a contactor similar to that used by Climeworks, estimating the productivity to be 2.28 kg/m^3/day and the specific equivalent work to be 2.16 MJ/kg. This study does not consider the co-adsorption of water in the feed stream in the process modelling, which has been shown to be a significant design factor in other work [30]. The co-adsorption of water affects the productivity of the system through cooperative co-adsorption with CO_2, and the energy usage through significant additional latent heat required for regeneration of the bed during the desorption step.

Stampi-Bombelli et al. [14] modelled an S-TVSA process and found, in their base-case, that the productivity of the system is 1.98 kg/m^3/day and the specific equivalent work is 7.4 MJ/kg. This study reports a somewhat low productivity, and correspondingly high energy usage. In this case, we would attribute the lower performance of the designed unit to the application of heuristic design guidelines, rather than the application of formal optimization techniques. To provide a formal comparison between systems designed using heuristic guidelines, and those designed using formal optimization, we present in Sect. 3.4 a systematic comparison between these two approaches—using the process model developed in this work as a basis for both approaches.

Finally, in Fig. 4b we also provide a shaded region corresponding to the estimated range of performance of a 50 tn/yr commercial demonstration unit built and operated by Climeworks. We estimate the productivity of the unit to be

17.1–40.7 kg/m^3/day, depending on the assumed contactor dimensions (1.5–2 m side length), and the specific equivalent work as 3.3–5.1 MJ/kg [20, 31]. These estimates are based on the performance of an operational DAC unit, rather than process modelling, and serve to demonstrate that current estimates of the performance of adsorption-based DAC using temperature-swing cycles are in the correct magnitude in terms of system productivity and specific equivalent work. Climeworks further report that the steam usage in their design corresponds to a molar steam ratio of SR $\leq$ 20 mol$_{H_2O}$/mol$_{CO_2}$. We observe that points on the Pareto front presented in Fig. 3a yield molar steam ratios in the range SR = 8.8–30.8 mol$_{H_2O}$/mol$_{CO_2}$. Therefore, we contend that the thermal requirement of steam for regeneration estimated in this study is moderate and reasonable.

Overall, we can see that the studies summarised above, including our own work, present a relatively good agreement in terms of the specific equivalent work required for DAC using APDES-NFC adsorbent. Excluding the study of [14], we observe maximum second law efficiencies in the range $\mu_{2law} = 21.7$–28.2%. This in strong agreement with the expected upper limit for DAC anticipated in previous work $(\mu_{2law} \leq 30\%)$ [20, 31]. However, we see significant variability arising in the estimation of process productivity (1.98–141 kg/m^3/day). Owing to the differences in methodology between the studies outlined above, we highlight that treatment of cooperative CO_2/H_2O co-adsorption and CO_2 sorption kinetics are central towards an accurate characterisation of system productivity. Given that the productivity of such systems is both highly uncertain, and notably low in all cases, we assert that significant research efforts need to be dedicated towards characterization of these phenomena in future experimental work to allow computational process design studies to improve their reliability.

3.4 Optimum operating points

In Fig. 5, we provide the distributions of the operating conditions used as decision variables for the operating points

on the process Pareto front (Fig. 3). The orange violin plots show the distribution of the decision variables on our Pareto front generated using the NSGA-II algorithm, and the solid blue lines correspond to the operating conditions specified from heuristic design guidelines (Sect. 3.3). Note that the ranges of the distributions in Fig. 5 have been re-scaled onto the interval [0, 1] to improve readability by applying the following transformation: $\theta \rightarrow (\theta - \theta_L)/(\theta_U - \theta_L)$ according to the variable bounds given in Table 3. Additionally, we also present the system productivity as a function of the operating conditions for the operating points on the process Pareto front in Section S.7 of the Supporting Information. We can see in Fig. 5 that the operating conditions specified for the heuristic design case lie outside of the optimal operating condition distributions for all operating conditions, except the desorption pressure (p_L) and the steam flowrate (v_s). Particularly, we can see that the heuristic rules used to determine the step durations ($t_{ads}, t_{heat}, t_{des}$) lead to rather sub-optimal decisions.

With respect to the adsorption time (t_{ads}), we can see that a significant loading of the adsorbent is favorable owing to the long adsorption times at optimality (in agreement with the corresponding heuristic guideline). We have observed from forward process simulations that the total adsorbed amount of CO_2 in the column tends to grow quite linearly until the sorbent is nearly fully saturated. Therefore, from the perspective of achieving a high average capture rate, it seems that it should always be optimal to proceed the adsorption step until a point of near-saturation of the adsorption bed. With respect to the desorption time (t_{des}), we can see in Fig. 5 that the optimal process operating points present substantially lower desorption times than that suggested heuristically. Again based on forward process simulations, we have observed that the total adsorbed amount of CO_2 in the column tends to decline in a strongly non-linear fashion throughout the desorption step. Initially, the rate of desorption is high and CO_2 is rapidly desorbed from the solid. However, as the desorption step continues, the desorption rate declines significantly. There is therefore a powerful diminishing returns effect displayed in the desorption step, wherein substantially longer desorption times do not lead to a significantly greater amount of CO_2 being recovered from the bed. Therefore, from the perspective of trying to attain the highest possible average rate of desorption, shorter desorption times are optimal. With respect to the heating time (t_{heat}), we see that the optimal heating time is larger than that from the design heuristic (i.e. that it is optimal to pre-heat the bed to more than the amount strictly required to prevent steam purge condensation). This is because, as described in Sect. 2.1, in addition to heating the bed, the heating step also helps to remove residual N_2 through a displacement effect due to vacuum level being maintained inside the column. Therefore, we can expect that longer heating times generally

correlate against achieving a higher CO_2 product purity during the subsequent desorption step.

The distributions of optimal desorption pressures (p_L) and steam temperatures (T_H) in Fig. 5 indicate that very low vacuum levels and high desorption temperatures are preferable for achieving efficient process performance. Here, we should note that the bounds on these operating conditions (Table 3) are physical, and therefore even though these operating conditions are at/near their respective bounds at optimality, we cannot credibly alter the bounds for the purpose of achieving better process performance. The lower bound on the desorption pressure is determined by the evacuation pressure which can be credibly achieved in an industrial-scale vacuum swing process [40], and the upper bound on the steam temperature is determined by the thermal stability characteristics of the adsorbent material. Finally, we see that for all operating conditions, except the steam flowrate (v_s), the distribution of optimal decisions is quite tight. This indicates that in the region of the operating condition space at/near optimal operation, the steam flowrate has dominant control over the trade-off between productivity and energy usage.

All of the above serves to underline the central need for applying formal optimization techniques when designing such a complex system, as simple design heuristics are not able to practically account for the large number of interrelated and non-linear factors which determine the relationship between each operating condition and the performance of the process.

4 Discussion

In Sect. 3.1, we found that the maximum productivity of the S-TVSA process using APDES-NFC adsorbent is very low $\left(\text{Pr}_{max} = 6.20\,\text{kg/m}^3/\text{day}\right)$. Such low productivity for the system would demand a large land footprint when deployed at large scales, challenging to the idea of co-locating DAC units to the infrastructure needed for the provision of energy, and CO_2 transport and storage, to enable environmental effectiveness. In the following, we explore the role of three key design parameters in determining the optimal productivity of the system, (1) the ambient air conditions, (2) the CO_2 sorption kinetics, and (2) the contactor design.

We have analyzed the effect of ambient conditions, CO_2 kinetics, and contactor design using a systematic approach. The effect of the ambient air conditions on the system performance is studied by varying the temperature $\left(T_a\right)$ and relative humidity $\left(r_H\right)$ of the feed stream. The effect of the CO_2 kinetics on the system performance is studied by varying the linear driving force (LDF) mass transfer coefficient for CO_2 sorption (k_{CO_2}). Finally, the effect of the contactor design is studied by varying the aspect ratio of the adsorption column.

We have defined the aspect ratio of the column through the length-to-radius ratio (τ) of the column, which is expressed as $\tau = L/r_{in}$.

In the following, we consider a wide range of possible system design cases by varying feed conditions, CO_2 kinetic constant, and contactor aspect ratio. For each considered design case, we calculate the optimal (maximum) productivity of the S-TVSA process. Different from previous studies, we consider the optimal process performance by conducting constrained single-objective productivity maximization for each considered design case. This is key to understand the system sensitivity to variable design parameters, as the process operating conditions which generate the best possible performance for each design case are likely to be substantially different. The optimization problem is formulated as follows:

$$\min_{\theta} -Pr + \phi$$
$$\text{s.t.} \quad \theta_L \leq \theta \leq \theta_U$$
$$\phi = 0.25 \times [\max(0, 95 - Pu_{CO_2})]^2$$

As in Sect. 3, we solve the optimization problem using the NSGA-II algorithm. Here, we apply the algorithm for 25 generations with a population size of 70. The operating conditions of the S-TVSA process used as decision variables, and their respective bounds, are identical to those used in Sect. 3 and are detailed in Table 3.

4.1 Effect of ambient air conditions

First, we study the effect of the ambient air conditions on the maximum achievable productivity of the S-TVSA process. We have optimized the system performance for 121 unique combinations of feed temperature (T_a) and relative humidity (r_H) in the ranges $T_a \in [5, 30]\,°C$ and $r_H \in [0, 100]\%$. These intervals represent a wide range of possible ambient conditions for which DAC processes may be expected to operate, including locations in Canada, Norway, Switzerland, the United Kingdom, and the United States [11]. In each optimization problem, the CO_2 sorption kinetics are fixed at $k_{CO_2} = 2 \times 10^{-4}\,s^{-1}$ and the contactor aspect ratio is fixed at $\tau = 1/8$, as in the nominal design case presented in Sect. 3. In Fig. 6, we present the maximum productivity of the system as a function of the ambient air conditions. The black crosses indicate the points in the (T_a, r_H) space at which productivity optimization was carried out, and the contour map corresponds to a surface fitted through the generated values of maximum system productivity, as there is some noise present in the optimization outputs owning to the stochastic nature of the NSGA-II algorithm used to optimize each design case.
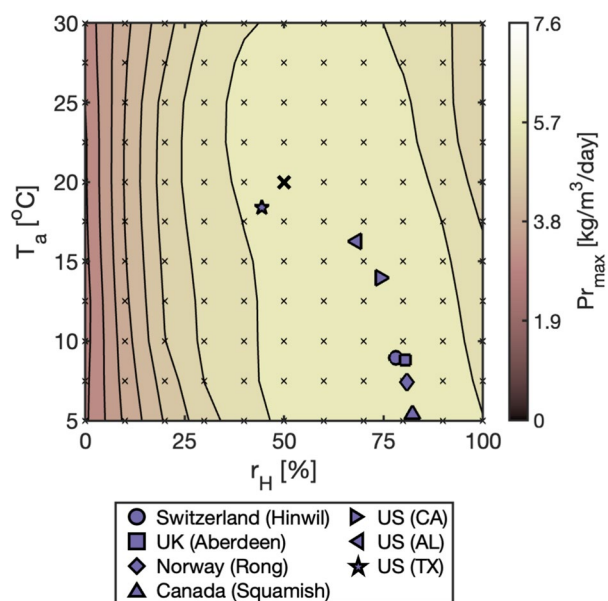

Fig. 6 Maximum productivity of the S-TVSA process as a function of the ambient air conditions (T_a, r_H). Black crosses correspond to the combinations of temperature and relative humidity used for constrained single-objective optimization using the NSGA-II algorithm to determine the maximum productivity. The bold black cross indicates the ambient conditions used in the base-case design preesented in Sect. 3 $(T_a = 20\,°C, r_H = 50\%)$. Purple symbols correspond to the annual average ambient conditions at seven locations where commercial demonstration DAC processes have been planned or constructed [11], including: Switzerland, the United Kingdom (UK), Norway, Canada, and the United States (US)

We can see that the contour lines in Fig. 6 are orientated roughly vertically, indicating that the relative humidity of the feed has the strongest effect on the maximum productivity. In the studied range of relative humidities, the maximum productivity varies by a factor of approximately 3-fold (2.24–6.41 kg/m³/day). The optimal range of relative humidity in the ambient air is approximately $r_H = 50$–75%. We hypothesize that a balance of two effects in the adsorption equilibrium behaviour of APDES-NFC yields this result. First, at low relative humidites, there is insufficient moisture in the feed gas to allow for significant amounts of co-operative adsorption with CO_2. Therefore, at low humidities, the uptake of CO_2 on the sorbent at the very low partial pressures at which CO_2 is present in the air is limited. This will lower the working capacity of the sorbent, and hence limit the productivity of the overall system. Conversely, at very high humidities, water adsorption begins to out-compete CO_2 adsorption and leads to a net reduction in the capacity of the system for adsorbing CO_2—causing a small decrease in the productivity. We note that this effect is particularly pronounced at higher temperatures, as CO_2 adsorption is suppressed at higher temperatures, while H_2O adsorption

is invariant with temperature at a given relative humidity (see Fig. 2).

We can see that the ambient temperature does not have a strong effect on the maximum productivity of the system. This behaviour is a consequence of the weak temperature dependence of the CO_2 isotherm for small temperature changes at/around ambient conditions. Therefore, although the ambient temperature will inevitably have an impact of the adsorption dynamics of the system, this impact is not large enough that it cannot be accommodated for by optimization of the system operating conditions. This result highlights the importance of considering *optimized* system performance when carrying out studies to assess the sensitivity of the system performance to design parameters.

The purple symbols in Fig. 6 indicate the annual average temperature and relative humidity at seven locations where commercial demonstration DAC processes have been planned or constructed, including: Switzerland (Climeworks, constructed), the United Kingdom (Carbon Engineering, planned), Norway (Carbon Engineering, planned), Canada (Carbon Engineering, under commission), and the United States (Global Thermostat, non-operational) [11]. We can see that all of the considered DAC processes have been sited in locations which fall within the highest maximum productivity region in the (T_a, r_H) space, making these ideal locations for the deployment of S-TVSA processes. For all locations, except US (TX), the average ambient conditions lie close to the centre of the highest maximum productivity region. This means that seasonal variability in the ambient conditions should be able to be accommodated by variation of the process operating conditions, for a fixed system design, without a significant impact on the process productivity.

4.2 Effect of CO_2 kinetics

Next, we study the effect of the CO_2 kinetic constant on the maximum achievable productivity of the S-TVSA process. We have optimized the system performance for 20 unique values of the CO_2 kinetic constant (k_{CO_2}) in the range $k_{CO_2} \in [2 \times 10^{-5}, 20]$ s^{-1}. This interval represents a wide range of possible kinetics for hypothetical adsorbents for DAC, where a value of $k_{CO_2} = 2 \times 10^{-5}$ s^{-1} corresponds to rather slow kinetics for a typical DAC sorbent, and a value of $k_{CO_2} = 20$ s^{-1} corresponds to very fast kinetics which would be more typical of applications of adsorption to post-combustion CO_2 capture. We note that for APDES-NFC adsorbent, the following values have previously been adopted in the literature: $k_{CO_2} = 2 \times 10^{-4}$ s^{-1} ([14], this work), $k_{CO_2} = 4 \times 10^{-3}$ s^{-1} [22], and $k_{CO_2} = 0.1$ s^{-1} [20]. In each optimization problem, the contactor aspect ratio is fixed
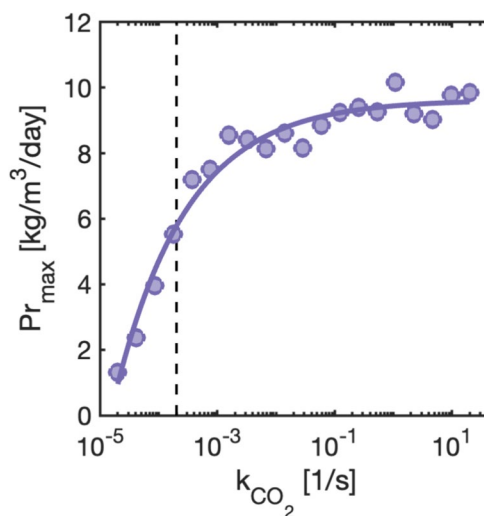

Fig. 7 Maximum productivity of the S-TVSA process as a function of the CO_2 kinetic constant (k_{CO_2}). Symbols correspond to the maximum productivity for each considered design case obtained by constrained single-objective optimization using the NSGA-II algorithm. The solid line corresponds to a trend line fitted through the generated points. The vertical dashed line indicates the kinetic constant used in the base-case design presented in Sect. 3 $\left(k_{CO_2} = 2 \times 10^{-4} \text{ s}^{-1}\right)$

at $\tau = 1/8$, and the ambient conditions are $T_a = 20\,°C$ and $r_H = 50\%$, as in the nominal design case presented in Sect. 3.

In Fig. 7, we present the maximum productivity of the system as a function of the CO_2 kinetic constant. Each symbol corresponds to the maximum productivity obtained by solution of the corresponding constrained single-objective optimization problem. The solid line corresponds to a trend line fitted to the generated points, as there is some noise present in the optimization outputs owning to the stochastic nature of the NSGA-II algorithm used to optimize each design case. We can see that initially, as the CO_2 kinetics get faster, the productivity of the system increases significantly. However, at a CO_2 kinetic constant of approximately $k_{CO_2} = 10^{-2}$ s^{-1}, there is a plateau in the productivity for increasing CO_2 kinetics. Therefore, we observe that using adsorbent materials with CO_2 kinetic constants $k_{CO_2} > 10^{-2}$ s^{-1} does not yield better process-scale performance. As in other adsorption-based separation systems, we hypothesise that there is a balance of two key effects occurring with respect to the relationship between the CO_2 kinetics and the system productivity. When the CO_2 kinetics are slow, using a sorbent with relatively faster kinetics will allow for quicker loading/unloading of the sorbent throughout the S-TVSA cycle, which will improve the system productivity by enabling shorter overall cycle times. However, when the CO_2 kinetics are much faster, thermal effects in the adsorption column become a strong controlling factor. Chemical adsorption of CO_2 onto the adsorbent

surface is a strongly exothermic process ($\Delta H = -57$ kJ/mol). Therefore, when the rate of adsorption becomes too high, the temperature in the column rises locally and is sustained for longer as the large rate of heat generation cannot be counteracted by a sufficient rate of heat dissipation. An exemplary profile of the evolution of the temperature computed at the outlet of the column is shown in Figure S8 of the Supporting Information for the operating point at fast kinetics ($k_{CO_2} = 2 \times 10^1$ s^{-1} with $Pr_{max} = 10$ kg/m^3/day) and at slow kinetics ($k_{CO_2} = 2 \times 10^{-5}$ s^{-1} with $Pr_{max} = 1.5$ kg/m^3/day). The results indicate that the higher kinetic case has a consistently higher temperature profile. As illustrated in Fig. 2, the equilibrium capacity of the sorbent is a strong decreasing function of increasing temperature. So, when the rate of sorption is high, a rapid rise in the local temperature acts to dampen the rate of further sorption by lowering the driving force for mass transfer between the gas- and adsorbed-phases. Similarly, we can understand that the same mechanism acts to dampen the achievable rate of desorption during the desorption step for the endothermic removal of CO_2 from the adsorbent surface. Based on these results, we contend that while searching for DAC sorbents with fast CO_2 kinetics is indeed a key design factor, there is a limit to the achievable performance at high CO_2 kinetics owing to thermal effects in the S-TVSA process.

4.3 Effect of contactor design

Finally, we have studied the effect of the contactor aspect ratio on the maximum achievable productivity of the S-TVSA process. We have optimized the system performance for 20 unique values of the contactor aspect ratio (τ) in the range $\tau \in [1/16, 6]$. For each considered contactor aspect ratio, we have conducted the optimization at 7 unique values of the CO_2 kinetic constant in the range $k_{CO_2} \in [2 \times 10^{-5}, 20]$ s^{-1}, to allow us to assess if the choice of optimal contactor design depends on the kinetics of the

chosen sorbent. The chosen range represents a wide variety of possible contactor designs, where a value of $\tau = 1/16$ is a very shallow "pancake-style" design, and a value of $\tau = 6$ is a long "column-style" design. We note that in Sect. 3, the nominal contactor aspect ratio was $\tau = 1/8$, which is a typical pancake-style design for DAC processes. The conventional argument adopted in previous studies to justify the use of a pancake-style contactor design is that the bed length needs to be small to allow for a low pressure drop in the column such that the electrical energy associated with processing large volumes of air in the adsorption step is low [14, 16]. However, we note that based on our own optimization results, and the results of previous studies, that for an S-TVSA process for DAC [14–16], the electrical energy usage represents only a small fraction of the overall energy duty of the process, with the majority of the energy duty being associated with the thermal burden of generating the steam purge for the desorption step. Therefore, we suggest that one should optimize the contactor aspect ratio with respect to mass transfer performance, rather than constraining the design based on heuristic arguments around the electrical energy usage.

In Fig. 8, we provide a schematic representation of contactor designs with aspect ratios of $\tau = 1/4$, $\tau = 1$, and $\tau = 3$. As we can see, the chosen range of contactor aspect ratios generates a wide range of designs, for which we can expect significantly distinct mass transfer characteristics. We note that for each considered contactor aspect ratio, the total column volume is fixed to that of the nominal design presented in Sect. 3 ($V_{bed} = 1.2 \times 10^{-3}$ m^3). This is because in this work we are interested to assess the impact of contactor design on the system performance, and not the effect of system scale. Therefore, to provide a fair basis of comparison between the different contactor designs, the scale of the system is constant between all the considered design cases. For each column aspect ratio, we set the outer column radius such that the thickness of the column wall is constant at $\Delta r = (r_{out} - r_{in}) = 0.017$ m.

Fig. 8 Schematic representation of contactor designs with aspect ratios of $\tau = 1/4$, $\tau = 1$, and $\tau = 3$. The contactor aspect ratio is defined as $\tau = L/r_{in}$. The column volume and wall thickness are constant for all contactor designs, at $V_{bed} = 1.2 \times 10^{-3}$ m^3 and $\Delta r = 0.017$ m, respectively
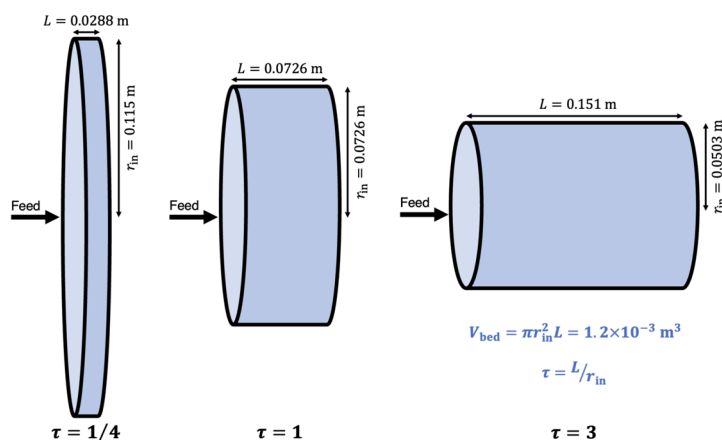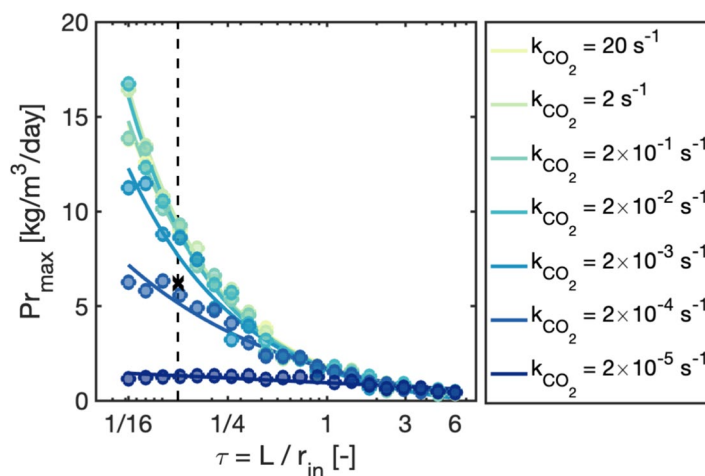
Fig. 9 Maximum productivity of the S-TVSA process as a function of the contactor aspect ratio (τ). The maximum productivity is calculated for each contactor aspect ratio at 7 unique CO_2 kinetic constants (k_{CO_2}), as indicted in the legend. Symbols correspond to the maximum productivity for each considered design case obtained by constrained single-objective optimization using the NSGA-II algorithm. The solid lines correspond to trend lines fitted to the generated points for each CO_2 kinetic constant. The vertical dashed line indicates the aspect ratio used in the base-case design presented in Sect. 3 ($\tau = 1/8$). The black cross corresponds to the base-case scenario presented in Sect. 3

In Fig. 9, we present the maximum productivity of the system as a function of the contactor aspect ratio. For each considered contactor aspect ratio, we calculate the maximum productivity for 7 unique values of the CO_2 kinetic constant. Each symbol corresponds to the maximum productivity obtained by solution of the corresponding constrained single-objective optimization problem. The solid lines correspond to trend lines fitted to the generated points for each CO_2 kinetic constant. As we can see, for the pancake-style designs (low τ), a higher CO_2 kinetic constant is favorable. Again, as shown in Fig. 7, we find that there is some upper limiting value to the productivity of the system for each contactor design, owing to thermal effects dominating the sorption dynamics at higher CO_2 kinetic constants. Further, we observe that in general as the length of the column is increased, the productivity of the system decreases. Given that the curves of maximum productivity as a function of the contactor aspect ratio collapse onto a single universal curve for all CO_2 kinetic constants at large values of the aspect ratio, we hypothesize that at high column aspect ratios the limiting factor to the sorption process is the driving force for mass transfer. For shorter column lengths, one can expose more of the sorbent at one time to the feed concentration (faster sorption towards equilibrium), which is more efficient in terms of cycle time. With a longer column, this process takes longer. Therefore, at larger aspect ratios, the CO_2 kinetic constant does not have significant control over the rate of sorption, as the driving force for mass transfer becomes too low for it to play a significant role in determining the system performance.

Based on these results, we can make several important observations. First, supporting the results presented in Fig. 7, improved CO_2 kinetics do help to improve the performance of the system. However, there is a limit to the available improvement based on thermal effects in the column. We observe that this limiting performance is a function of the aspect ratio of the column, where lower aspect ratios are favorable for higher productivity, but that the transition from a mass transfer dominated regime to a heat transfer dominated regime, in terms of CO_2 kinetics, does not vary strongly as a function of the aspect ratio. Second, we observe that while pancake-style designs do indeed offer better overall system performance in terms of the productivity, sufficiently fast CO_2 kinetics are required to access this regime of improved performance. Particularly, we see in Fig. 9 that for a CO_2 kinetic constant of $k_{CO_2} = 2 \times 10^{-5}$ s^{-1} that the optimal performance of the process is essentially invariant with the aspect ratio of the contactor. Third, we note that from the perspective of achieving efficient heat transfer in the system from the heating jacket to the adsorbent bed, column-style designs are strongly preferable as they have higher surface area to volume ratios. Therefore, in the design case of an adsorbent with relatively slow kinetics, it is likely preferable from a practical perspective to deploy a column-style design. Additionally, we note that the kinetics of sorbents for DAC applications are scarcely available in the current literature. Therefore, process design exercises may wish to proceed in the short-term using column-style designs to allow for greater confidence in

the process-scale performance in the absence of accurate data for the sorption kinetics. Such an approach will significantly reduce the risk of overestimating the optimal system performance. Finally, it is worth noting that these results have been obtained from the solution of a single-objective productivity maximisation problem. Because of the trade-off between productivity and specific equivalent work (Fig. 3), one expects that the observed increase in productivity comes at the expense of an increased energy usage of the DAC unit. An example of this trade-off is presented in Figure S9 of the Supporting Information for the nominal case with kinetic constant $k_{CO_2} = 2 \times 10^{-4}$ s^{-1}. The plot of W_{eq} vs. log(τ) indicates the presence of a minimum at an aspect ratio of approx. 1/4.

5 Conclusions

We have carried out the simulation and optimization of a 5-step steam-assisted temperature-vacuum swing adsorption (S-TVSA) process for purification of CO_2 from ambient air with an application to direct air capture (DAC). We have developed a state-of-the-art high fidelity dynamic process simulator for S-TVSA processes via finite volume simulation of the governing material, momentum, and energy balance equations subject to cyclic boundary conditions. We further couple the simulation to a thermo-dynamic process model of the equipment downstream of the adsorption column for the separation of CO_2/H_2O in the product gas by condensation. The simulator is coupled to a black-box optimization framework utilizing the non-dominated sorting genetic algorithm II (NSGA-II) to identify the optimal process performance for DAC on a fixed bed of APDES-NFC adsorbent based on maximizing the system productivity and minimizing the system energy usage, subject to achieving high CO_2 purity ($\geq$95%). We find that the maximum productivity of the process is $Pr_{max} = 6.20$ kg/m^3/day and the minimum energy usage is $W_{EQ,min} = 1.66$ MJ/kg. The minimum energy usage is comparable in magnitude to the application of adsorption-based separations to other CO_2 capture applications, with the majority of the energy usage for the process being associated with the thermal burden of generating the steam purge for the desorption step. We have found that heuristic design guidelines used to determine the process operating conditions in previous work are strongly sub-optimal, and lead to a significant underestimation of the potential process performance. As compared to a heuristic design case, the optimized process design achieves a $+629$% improvement in the system productivity and a -90.2% reduction in the system energy usage. We therefore contend that formal optimization is an essential cornerstone to the design of such complex systems.

The maximum productivity of the system is found to be very low, which would lead to a large required primary land footprint if such a process were to be deployed at climate-relevant scales. To understand the limiting factors to the optimal productivity of the system, we have conducted case studies considering design cases where we vary the ambient air conditions, CO_2 sorption kinetics, and contactor aspect ratio. With respect to the ambient air conditions, we find that moderate relative humidities (50–75%) are favourable for improved system productivity, by striking a balance between cooperative CO_2/H_2O adsorption, and competitive adsorption effects. A wide range of feed temperatures (5–30 °C) can be accommodated by a fixed design through optimization of the process operating conditions without a significant impact on the productivity of the process. We find that improved CO_2 kinetics are able to significantly improve the system productivity, but that at very high CO_2 kinetics the performance of the process becomes constrained by thermal effects in the adsorption column. We have observed that the productivity of the system is invariant with the CO_2 kinetics for column-style contactor designs, owing to mass transfer driving force constraints for such designs. On the contrary, we find that pancake-style contactor designs offer potential benefits in terms of system productivity. However, the performance improvements offered by the pancake-style design require that the CO_2 kinetics are sufficiently fast. A further analysis of factors, such as feed flow distribution and heating or cooling constraints, is needed to truly assess the potential of pancake-style configurations at pilot or industrial scale.

The results herein demonstrate that there is a strong degree of synergy which needs to be achieved between geographical siting, adsorbent selection, contactor design, and process operating conditions to achieve environmentally efficient DAC processes with low energy usage and low land footprint. Future work should therefore aim to employ, wherever possible, high fidelity process modelling and formal optimization tools to enable accurate process performance characterization and identification of optimal process designs for DAC.

Data availability The data that support the findings of this study are available from the corresponding author, RP, upon reasonable request.

Declarations

Conflict of interest The authors declare that they have no conflict of interest.

Ethical approval Not applicable.

Open Access This article is licensed under a Creative Commons Attribution 4.0 International License, which permits use, sharing, adaptation, distribution and reproduction in any medium or format, as long as you give appropriate credit to the original author(s) and the source, provide a link to the Creative Commons licence, and indicate if changes were made. The images or other third party material in this article are included in the article's Creative Commons licence, unless indicated otherwise in a credit line to the material. If material is not included in the article's Creative Commons licence and your intended use is not permitted by statutory regulation or exceeds the permitted use, you will need to obtain permission directly from the copyright holder. To view a copy of this licence, visit http://creativecommons.org/licenses/by/4.0/.

References

1. IPCC: Climate change 2021: The physical science basis. Working group I contribution to the sixth assessment report of the intergovernmental panel on climate change (2021)
2. IEA: Direct air capture: a key technology for net zero (2022)
3. Ozkan, M., Nayak, S.P., Ruiz, A.D., Jiang, W.: Current status and pillar of direct air capture technologies. iScience **25**, 103990 (2022). https://doi.org/10.1016/j.isci.2022.103990
4. Erans, M., Sanz-Perez, E.S., Hanak, D.P., Clulow, Z., Reiner, D.M., Mutch, G.A.: Direct air capture: process technology, techno-economic and socio-polotical challenges. Energy Environ. Sci. **15**, 1360–1405 (2022). https://doi.org/10.1039/D1EE03523A
5. McQueen, N., Gomes, K.V., McCormick, C., Bluemanthal, K., Pisciotta, M., Wilcox, J.: A review of direct air capture (DAC): scaling up commercial technologies and innovating for the future. Prog. Energy **3**, 032001 (2021). https://doi.org/10.1088/2516-1083/abf1ce
6. Krevor, S., Coninck, H., Gasda, S.E., Ghaleigh, N.S., Gooyert, V., Hajibeygi, H., Juanes, R., Neufeld, J., Roberts, J.J., Swennenhuis, F.: Subsurface carbon dioxide and hydrogen storage for a sustainable energy future. Nat. Rev. Earth Environ. **4**, 102–118 (2023). https://doi.org/10.1038/s43017-022-00376-8
7. Artz, J., Muller, T.E., Thenert, K., Kleinekorte, J., Meys, R., Sternberg, A., Bardow, A., Leitner, W.: Sustainable conversion of carbon dioxide: an integrated review of catalysis and life cycle assessment. Chem. Rev. **118**, 434–504 (2018). https://doi.org/10.1021/acs.chemrev.7b00435
8. Liu, C.M., Sandhu, N.K., McCoy, S.T., Bergerson, J.A.: A life cycle assessment of greenhouse gas emissions from direct air capture and Fischer–Tropsch fuel production. Sustain. Energy Fuels **4**, 3129–3142 (2020). https://doi.org/10.1039/c9se00479c
9. Deutz, S., Bardow, A.: Life-cycle assessment of an industrial direct air capture process based on temperature-vacuum swing adsorption. Nat. Energy **6**, 203–213 (2021). https://doi.org/10.1038/s41560-020-00771-9
10. Zhu, X., Xie, W., Wu, J., Miao, Y., Xiang, C., Chen, C., Ge, B., Gan, Z., Yang, F., Zhang, M., O'Hare, D., Li, J., Ge, T., Wang, R.: Recent advances in direct air capture by adsorption. Chem. Soc. Rev. **51**, 6574–6651 (2022). https://doi.org/10.1039/D1CS00970B
11. Low, M.-Y.A., Barton, L.V., Pini, R., Petit, C.: Analytical review of the current state of knowledge of adsorption materials and processes for direct air capture. Chem. Eng. Res. Des. **189**, 745–767 (2023). https://doi.org/10.1016/j.cherd.2022.11.040
12. Sinha, A., Darunte, L.A., Jones, C.W., Realff, M.J., Kawajiri, Y.: Systems design and economic analysis of direct air capture of CO_2 through temperature vacuum swing adsorption using MIL-101(Cr)-PEI-800 and mmen-Mg2(dobpdc) MOF adsorbents. Ind. Ind. Eng. Chem. Res. **56**, 750–764 (2017). https://doi.org/10.1021/acs.iecr.6b03887
13. Sinha, A., Realff, M.J.: A parametric study of the techno-economics of direct CO_2 air capture systems using solid adsorbents. AIChE J. **65**, e16607 (2019). https://doi.org/10.1002/aic.16607
14. Stampi-Bombelli, V., Spek, M., Mazzotti, M.: Analysis of direct capture of CO_2 from ambient air via steam-assisted temperature-vacuum swing adsorption. Adsorption **26**, 1183–1197 (2020). https://doi.org/10.1007/s10450-020-00249-w
15. Zhu, X., Ge, T., Yang, F., Wang, R.: Design of steam-assisted temperature vacuum-swing adsorption processes for efficient CO_2 capture from ambient air. Renew. Sustain. Energy Rev. **137**, 110651 (2021). https://doi.org/10.1016/j.rser.2020.110651
16. Young, J., Mcilwaine, F., Smit, B., Garcia, S., Spek, M.: Process-informed adsorbent design guidelines for direct air capture. Chem. Eng. J. **456**, 141035 (2023). https://doi.org/10.1016/j.cej.2022.141035
17. Climeworks: United States Patent Application (US 2017/1006330 A1) (2017)
18. GlobalThermostat: United States Patent Application (US 2017/0361271 A1) (2017)
19. Haghpanah, R., Majumder, A., Nilam, R., Rajendran, A., Farooq, S., Karimi, I.A., Amanullah, M.: Multiobjective optimization of a four-step adsorption process for postcombustion CO_2 capture via finite volume simulation. Ind. Eng. Chem. Res. **52**, 4229–4265 (2013). https://doi.org/10.1021/ie302658y
20. Sabatino, F., Grimm, A., Gallucci, F., Sint Annaland, M., Kramer, G.J., Gazzani, M.: A comparative energy and costs assessment and optimization for direct air capture technologies. Joule **5**, 2047–2076 (2021). https://doi.org/10.1016/j.joule.2021.05.023
21. Schellevis, H.M., Combe, J.D., Brilman, D.W.F.: An optimization framework for a temperature-vacuum swing adsorption direct air capture process (November 30, 2022). In: Proceedings of the 16th International Conference on Greenhouse Gas Control Technologies Conference (GHGT-16) 23–24 Oct (2022). https://doi.org/10.2139/ssrn.4290070
22. Leonzio, G., Fennell, P.S., Shah, N.: A comparative study of different sorbents in the context of direct air capture (DAC): evaluation of key performance indicators and comparisons. Appl. Sci. **12**, 2618 (2022). https://doi.org/10.3390/app12052618
23. Gebald, C., Wurzbacher, J.A., Borgschulte, A., Zimmermann, T., Steinfeld, A.: Single-component and binary CO_2 and H_2O adsorption on amine functionalized cellulose. Environ. Sci. Technol. **48**, 2497–2504 (2014). https://doi.org/10.1021/es404430g
24. Wurzbacher, J.A., Gebald, C., Piatkowski, N., Steinfeld, A.: Concurrent separation of CO_2 and H_2O from air by a temperature-vacuum swing adsorption/desorption cycle. Environ. Sci. Technol. **46**, 9191–9198 (2012). https://doi.org/10.1021/es301953k
25. Wurzbacher, J.A., Gebald, C., Brunner, S., Steinfeld, A.: Heat and mass transfer of temperature-vacuum swing desorption for CO_2 capture from air. Chem. Eng. J. **283**, 1329–1338 (2016). https://doi.org/10.1016/j.cej.2015.08.035
26. Ward, A., Pini, R.: Integrated uncertainty quantification and sensitivity analysis of single-component dynamic column breakthrough

experiments. Adsorption **28**, 161–183 (2022). https://doi.org/10.1007/s10450-022-00361-z

27. Ward, A., Pini, R.: Efficient Bayesian optimization of industrial-scale pressure-vacuum swing adsorption processes for CO_2 capture. Ind. Eng. Chem. Res. **61**, 13650–13668 (2022). https://doi.org/10.1007/s10450-022-00361-z

28. Li, G., Xiao, P., Webley, P., Zhang, J.: Capture of CO_2 from high humidity flue gas by vacuum swing adsorption with Zeolite 13x. Adsorption **14**, 415–422 (2008). https://doi.org/10.1007/s10450-007-9100-y

29. Danaci, D., Webley, P.A., Petit, C.: Guidelines for techno-economic analysis of adsorption processes. Front. Chem. Eng. **2**, 602430 (2021). https://doi.org/10.3389/fceng.2020.602430

30. Young, J., Garcia-Diez, E., Garcia, S., Spek, M.: The impact of binary water-CO_2 isotherm models on the optimal performance of sorbent-based direct air capture processes. Energy Environ. Sci. **14**, 5377–5394 (2021). https://doi.org/10.1039/d1ee01272j

31. Herzog, H.: In: Bui, M., Mac Dowell, N. (eds.) The Royal Society of Chemistry, vol. 6, pp. 115–137. Greenhouse Gas Removal Technologies (2022)

32. Rajagopalan, A.K., Rajendran, A.: The effect of nitrogen adsorption on vacuum swing adsorption based post-combustion CO_2 capture. Int. J. Greenh. Gas Control **78**, 437–447 (2018). https://doi.org/10.1016/j.ijggc.2018.09.002

33. Balashankar, V.S., Rajendran, A.: Process optimization-based screening of zeolites for post-combustion CO_2 capture by vacuum swing adsorption. Sustain. Chem. Eng. **7**, 17747–17755 (2019). https://doi.org/10.1021/acssuschemeng.9b04124

34. Krishnamurthy, S., Boon, J., Grande, C., Lind, A., Blom, R., Boer, R., Willemsen, H., Scheemaker, G.: Screening supported amine sorbents in the context of post-combustion carbon capture by vacuum swing adsorption. Chemie Ingenieur Technik **93**, 929–940 (2021). https://doi.org/10.1002/cite.202000172

35. Peh, S.B., Farooq, S., Zhao, D.: A metal-organic framework (MOF)-based temperature swing adsorption cycle for postcombustion CO_2 capture from wet flue gas. Chem. Eng. Sci. **250**, 117399 (2022). https://doi.org/10.1016/j.ces.2021.117399

36. Grossmann, Q., Stampi-Bombelli, V., Yakimov, A., Docherty, S., Coperet, C., Mazotti, M.: Developing versatile contactors for direct air capture of CO_2 through amine grafting onto alumina pellets and alumina wash-coated monoliths. Ind. Eng. Chem. Res. **62**, 13594–13611 (2023). https://doi.org/10.1021/acs.iecr.3c01265

37. Khurana, M., Farooq, S.: Adsorbent screening for post-combustion CO_2 capture: a method relating equilibrium isotherm characteristics to an optimum vacuum swing adsorption process performance. Ind. Eng. Chem. Res. **55**, 2447–2460 (2016). https://doi.org/10.1021/acs.iecr.5b04531

38. Breyer, C., Fasihi, M., Bajamundi, C., Creutzig, F.: Direct air capture of CO_2: a key technology for ambitious climate change mitigation. Joule **3**, 2053–2065 (2019). https://doi.org/10.1016/j.joule.2019.08.010

39. Kung, L., Aeschlimann, S., Charalambous, C., McIlwaine, F., Young, J., Shannon, N., Strassel, K., Maesano, C.N., Kahsar, R., Pike, D., Spek, M., Garcia, S.: A roadmap for achieving scalable, safe, and low-cost direct air carbon capture and storage. Energy Environ. Sci. **16**, 4280–4304 (2023). https://doi.org/10.1039/D3EE01008B

40. Krishnamurthy, S., Rao, V.R., Guntuka, S., Sharratt, P., Haghpanah, R., Rajendran, A., Amanullah, M., Karimi, I.A., Farooq, S.: CO_2 capture from dry flue gas by vacuum swing adsorption: a pilot plant study. AIChE J. **60**(5), 1830–1842 (2014)